IAI Journals.ASM.org

Impaired Early Cytokine Responses at the Site of Infection in a Murine Model of Type 2 Diabetes and Melioidosis Comorbidity

Kelly A. Hodgson,[a] Brenda L. Govan,[a] Anna K. Walduck,[b] Natkunam Ketheesan,[a] Jodie L. Morris[a]

Infectious Diseases and Immunopathogenesis Research Group, School of Veterinary and Biomedical Sciences, James Cook University, Townsville, Queensland, Australia[a]; School of Applied Sciences, RMIT University, Bundoora, Victoria, Australia[b]

Bacterial infections are a common and serious complication of type 2 diabetes (T2D). The prevalence of melioidosis, an emerging tropical infection caused by the Gram-negative bacterium *Burkholderia pseudomallei*, is increased in people with T2D. This is the first study to compare murine models of T2D and melioidosis. Susceptibility and disease progression following infection with *B. pseudomallei* were compared in our diet-induced polygenic mouse model and a leptin receptor-deficient monogenic model of T2D. The metabolic profile of mice with diet-induced diabetes, including body weight, blood glucose, cholesterol, triglycerides, insulin resistance, and baseline levels of inflammation, closely resembled that of clinical T2D. Following subcutaneous infection with *B. pseudomallei*, bacterial loads at 24 and 72 h postinfection in the blood, spleen, liver, lungs, and subcutaneous adipose tissue (SAT) at the site of infection were compared in parallel with the expression of inflammatory cytokines and tissue histology. As early as 24 h postinfection, the expression of inflammatory (interleukin-1β [IL-1β], tumor necrosis factor alpha [TNF-α], and IL-6) and T_H1 (IL-12 and gamma interferon [IFN-γ]) cytokines was impaired in diabetic mice compared to nondiabetic littermates. Early differences in cytokine expression were associated with excessive infiltration of polymorphonuclear neutrophils (PMN) in diabetic mice compared to nondiabetic littermates. This was accompanied by bacteremia, hematogenous dissemination of bacteria to the lungs, and uncontrolled bacterial growth in the spleens of diabetic mice by 72 h postinfection. The findings from our novel model of T2D and melioidosis comorbidity support the role of impaired early immune pathways in the increased susceptibility of individuals with T2D to bacterial infections.

Type 2 diabetes (T2D) continues to be a global health priority, driven by the aging population, obesity, dietary changes, and sedentary lifestyles (1). A significant yet underappreciated complication of T2D is the increased susceptibility to bacterial infections, which accounts for a considerable proportion of morbidity and mortality (2). T2D is the most common risk factor for melioidosis, an emerging bacterial infection in the tropics and subtropical regions (3–5). Caused by the intracellular Gram-negative bacterium *Burkholderia pseudomallei*, melioidosis typically presents as a febrile illness with concomitant pneumonia (6). The disease is difficult to diagnose, is inherently resistant to antibiotic therapy, and frequently results in septic shock with an unacceptably high mortality rate regardless of treatment (7).

The incidence of melioidosis is continuing to increase with the rising prevalence of T2D in regions of hyperendemicity. Currently up to 42% of patients with melioidosis in Australia (8, 9), 60% of patients in Thailand (10), and 76% of patients in India (11) have preexisting T2D. Melioidosis patients with comorbid T2D frequently develop acute pneumonia and bacteremia, which are associated with high mortality rates compared to those from other forms of the disease (9, 12). This significant association between T2D and severe bacterial infections such as melioidosis underscores the need for novel therapeutic strategies targeted to populations at risk. This will be facilitated by understanding the pathogenic mechanisms governing disease progression in susceptible hosts, providing impetus for the development of suitable models of comorbidity.

Cellular immune defects associated with T2D undoubtedly contribute to the increased susceptibility of patients with comorbid melioidosis. Impairments in phagocytosis and migration of polymorphonuclear neutrophils (PMN) from individuals with T2D in response to *B. pseudomallei* have previously been documented *in vitro* (13). Recently, using a human whole-blood model of melioidosis and comorbid T2D, we demonstrated that altered early cellular interactions of PMN and monocytes with *B. pseudomallei* underpin the increased susceptibility of individuals with T2D to melioidosis, particularly those with poorly controlled glycemia (14). An animal model of melioidosis and comorbid T2D is essential for *in vivo* characterization of host-pathogen interactions in the initial stages of infection, since the early immune pathways triggered are critical in determining disease progression.

Murine models have contributed significantly to our understanding of the immunopathogenesis of melioidosis and host protective responses toward *B. pseudomallei* (15–17). Defective function of bone-marrow derived dendritic cells (BMDC) and peritoneal elicited macrophages (PEC) in response to *B. pseudomallei* has previously been described using a streptozotocin-induced rodent model of type 1 diabetes (T1D) (18, 19). However, this model received criticism because the majority of patients with melioidosis have T2D (5), which has an etiology and pathogenesis distinct from those of T1D. One of the most widely used models of T2D is the leptin signaling-deficient *Dock7*^{m} *Lepr*^{db} mice (20). We

Received 30 August 2012 **Returned for modification** 15 October 2012
Accepted 21 November 2012
Published ahead of print 3 December 2012
Editor: B. A. McCormick
Address correspondence to Kelly A. Hodgson, Kelly.Hodgson@my.jcu.edu.au.
Supplemental material for this article may be found at http://dx.doi.org/10.1128/IAI.00930-12.

doi:10.1128/IAI.00930-12

have previously used BKS.Cg-*Dock7*^{m} +/+ *Lepr*^{db}/J mice as a murine model of T2D and comorbid melioidosis (21); however, the model is still limited by inconsistencies with clinical disease (20). Diet-induced models of T2D closely resemble clinical etiology; however, there are large discrepancies in reported phenotypes, complicated by differences in diet composition and period of feeding, together with the rodent strain and gender (22).

The aim of the current study was to develop a murine model reflective of T2D to enable *in vivo* characterization of early immune responses and disease progression following infection with *B. pseudomallei*. We compared monogenic and polygenic models of T2D using leptin signaling-deficient and high-fat-diet-fed (HFD) mice, respectively. While both models developed hyperinsulinemia and impaired glucose tolerance, we selected the polygenic model for all subsequent experiments since it closely reflects the etiology of T2D and is consistent with the World Health Organization (WHO) criteria for clinical T2D (23). Increased susceptibility of diabetic mice to *B. pseudomallei* infection was associated with defects in the inflammatory immune response after 24 h. The current study describes the first model of diet-induced T2D and melioidosis comorbidity and will serve as a valuable tool for further analysis of defects in early immune response pathways underlying contrasting disease progression in diabetic and nondiabetic hosts following infection with *B. pseudomallei*.

MATERIALS AND METHODS

Mice. A monogenic model and a polygenic model of T2D were compared to determine the most suitable model based on clinical criteria of T2D, which center on the development of hyperglycemia and insulin resistance (23). C57BL/6 mice have been extensively characterized as a model for chronic melioidosis. We therefore used C57BL/6J-*Dock7*^{m} *Lepr*^{db}/++ mice as a monogenic model of T2D. A genetic mutation in the leptin receptor causes homozygotes (*db/db*) to develop obesity, insulin resistance, and hyperglycemia. Heterozygous (*db/+*) littermates are lean and euglycemic and were used as littermate controls. Mice received standard rodent chow and water *ad libitum*.

Male 6- to 8-week-old C57BL/6 mice were randomly allocated to 2 dietary groups for the polygenic model. One group received *ad libitum* access to a high-fat (40% of energy) diet (SF00-219 Western diet; Specialty Feeds, Australia). This diet resembles typical dietary intakes of fat (33% of energy) in developed nations (24). Paired control mice received isometric quantities of standard rodent chow (12% of energy from fat; Specialty Feeds, Australia). HFD mice developed dyslipidemia, insulin resistance, and hyperglycemia and, based on these key diagnostic criteria for T2D, were subsequently selected for further characterization. Experiments were carried out in accordance with National Health and Medical Research Council guidelines and were approved by the institutional ethics committee (A1556).

Circulating metabolic, biochemical, and cytokine profiles. Blood glucose, total cholesterol, and triglycerides from the lateral tail vein ($n = 5$ per group) were measured for the duration of the study (Accutrend Plus Cobas; Roche Diagnostics, Germany). A glucose tolerance test was performed on 6-h-fasted mice ($n = 3$ per group) at 0, 15, 30, 60, and 120 min following intraperitoneal glucose challenge (2 g/kg body weight). Serum ($n = 5$ per group) was collected to determine the circulating levels of adipokines, including insulin, interleukin-6 (IL-6), and monocyte chemotactic protein 1 (MCP-1) (Milliplex MAP; Millipore) according to the manufacturer's instructions.

Infection with *B. pseudomallei*. *Burkholderia pseudomallei* (NCTC13178) was cultured and brought to logarithmic phase as previously described (25). After 20 weeks of diet intervention, mice ($n = 25$ per group) were inoculated subcutaneously with *B. pseudomallei* (4.9×10^5 CFU). The concentration was determined spectrophotometrically prior to administration and the dose confirmed retrospectively by plating on Ashdown agar. Uninfected control mice ($n = 5$ per group) received injections of phosphate-buffered saline (PBS) only. At 24 and 72 h postinfection, mice ($n = 10$ per group) were sacrificed to collect liver, lungs, spleen, blood, and subcutaneous adipose tissue (SAT) at the site of infection. The organs were bisected to enable determination of bacterial loads in parallel with cytokine expression or were frozen in liquid nitrogen for histological processing.

Organ cytokine expression. Immediately after removal, bisected organs were frozen in liquid nitrogen and stored at −70°C until processing in TRIzol (Invitrogen) according to the manufacturer's instructions. Total RNA was purified using innuPREP RNA columns (Analytik Jena, Germany), and RNA yield and purity were determined using a NanoDrop spectrophotometer (NanoDrop Technologies). RNA samples (1 μg) were incubated with DNase I (Invitrogen, Australia) to remove potential DNA contaminants and reverse transcribed with Moloney murine leukemia virus (MMLV) high-performance reverse transcriptase (AllianceBio) and oligo(dT) primers (Sigma-Aldrich, USA). Real-time quantitative PCR (qPCR) mixtures (20 μl) with 1× Immomix (Bioline, Australia), 1 μl template cDNA, and 0.4 μM primers (Sigma-Aldrich) were assayed in duplicate together with nontemplate controls using Rotor-Gene 6000 (Corbett Research, Australia) with Syto 9 (Molecular Probes) for detection of double-stranded DNA (dsDNA). Cycling conditions comprised polymerase activation at 95°C for 10 min followed by 40 cycles of 95°C for 10 s, 60°C for 15 s, and 72°C for 20 s. Product specificity was confirmed by melting curve analysis from 65°C to 99°C.

Primer pairs were designed with Primer3 software (26) to span exon boundaries, and the specificity was confirmed by BLAST analysis (see Table S1 in the supplemental material) (27). Standard curves with 5 serial dilutions were produced for each gene using purified DNA template to determine PCR efficiency for each primer set with real-time qPCR analysis software, version 6.0 (Corbett Life Science). Fold changes in cytokine expression were determined by the efficiency-corrected quantification model described previously (28) and normalized to the geometric mean after validation of the most stable reference genes (the peptidylprolyl isomerase B [PPIB] and β-actin genes) as described previously (29).

Histology. Tissues were frozen in OCT medium (Tissue Tek, The Netherlands) in liquid nitrogen. Cryosections (5 μm) were fixed in 10% buffered formalin for 10 min, followed by hematoxylin and eosin staining for histopathological examination or oil red O and hematoxylin counterstaining for determination of ectopic lipid accumulation. To visualize bacteria, sections were fixed in acetone for 10 min and permeabilized with 0.1% saponin before staining with anti-*B. pseudomallei* outer membrane protein (OMP) antibody followed by secondary horseradish peroxidase–anti-rabbit IgG and tyramide-Alexa Fluor 594 (TSA detection kit; Invitrogen, Australia). Sections were counterstained with DAPI (4′,6′-diamidino-2-phenylindole) (Vectashield mounting medium with DAPI; Vector Laboratories) and images acquired with a Zeiss laser scanning confocal microscope (LSM 700).

Statistical analysis. Statistical analysis was performed using IBM SPSS Statistics version 19. Kaplan-Meier survival curves were used to compare susceptibility to subcutaneous infection with *B. pseudomallei* between diabetic and nondiabetic mice. Body weight gain and glucose tolerance tests were compared by two-way repeated-measures analysis of variance (ANOVA). All other data were compared by unpaired Student *t* tests. Comparisons were considered to be significant at a *P* value of ≤0.05. Data were expressed as mean ± standard error (SE).

RESULTS

Characterization of a monogenic and polygenic model of T2D. Compared to heterozygous *db/+* mice, homozygous *db/db* mice had greater total body mass and adipose tissue ($P < 0.0001$) (Table 1). This was attributed to the increased daily energy intake, which was 40% higher in *db/db* mice than in *db/+* mice ($P =$

TABLE 1 Comparison of monogenic and polygenic murine models of type 2 diabetes

Parameter (unit)[a]	C57BL/6J-*Dock7*^{m} *Lepr*^{db}/++ model			Diet-induced C57BL/6 model		
	db/db	*db/+*	Significance[b]	HFD[c]	Control	Significance
Metabolic profile						
Body wt (g)	33.4 ± 0.64	21.3 ± 1.31	$P < 0.0001$*	28.4 ± 1.54	21.7 ± 1.04	$P = 0.007$*
Visceral AT (g)	2.107 ± 0.089	0.235 ± 0.009	$P < 0.0001$*	0.818 ± 0.155	0.161 ± 0.017	$P = 0.013$*
Subcutaneous AT (g)	0.368 ± 0.039	0.094 ± 0.009	$P < 0.0001$*	0.267 ± 0.044	0.095 ± 0.013	$P = 0.006$*
Liver (g)	2.536 ± 0.201	1.030 ± 0.027	$P = 0.002$*	1.317 ± 0.108	0.929 ± 0.068	$P = 0.016$*
Daily energy consumption (kJ/mouse)	79.1 ± 4.0	45.4 ± 2.7	$P = 0.002$*	53.0 ± 3.3	37.8 ± 2.1	$P = 0.018$*
Blood biochemical profile						
Cholesterol (mmol/liter)	3.00 ± 0.50	1.80 ± 0.21	$P = 0.056$ (NS)	4.14 ± 0.41	2.09 ± 0.10	$P = 0.006$*
Triglycerides (mmol/liter)	1.18 ± 0.16	0.85 ± 0.08	$P = 0.102$ (NS)	0.89 ± 0.09	0.60 ± 0.09	$P = 0.030$*
Glucose (mmol/liter)	12.4 ± 1.31	8.2 ± 0.85	$P = 0.054$ (NS)	9.7 ± 0.87	6.60 ± 0.25	$P = 0.026$*
Insulin (pg/ml)	12266 ± 1635	4117 ± 983	$P = 0.003$*	903 ± 240	212 ± 48	$P = 0.016$*
Insulin resistance (AUC[d])	2642 ± 492	1065 ± 177	$P = 0.039$*	1685 ± 117	880 ± 32	$P = 0.003$*
Inflammatory profile						
MCP-1 (pg/ml)	68.53 ± 17.30	16.09 ± 6.18	$P = 0.021$*	33.53 ± 8.26	19.04 ± 4.11	$P = 0.137$ (NS)
IL-6 (pg/ml)	79.36 ± 16.63	21.19 ± 4.69	$P = 0.022$*	23.15 ± 1.77	10.44 ± 0.56	$P = 0.003$*
TNF-α (relative mRNA expression in AT)	1.56 ± 0.504	0.340 ± 0.070	$P = 0.098$ (NS)	2.19 ± 0.500	1.01 ± 0.070	$P = 0.033$*

[a] Values are means ± standard errors.
[b] *, significant; NS, not significant.
[c] HFD, high-fat-diet-fed mice.
[d] AUC, area under glucose concentration-time curve.

0.003) (Table 1), due to hyperphagia. Weight gain was accompanied by severe insulin resistance ($P = 0.039$) (see Fig. S1 in the supplemental material) and subsequent hyperinsulinemia ($P = 0.003$) (Table 1). However, the increase in blood glucose was variable in *db/db* mice compared to *db/+* mice, and the difference was not statistically significant ($P = 0.054$) (Table 1). Circulating cholesterol and triglyceride levels were comparable between littermates ($P = 0.056$ and $P = 0.102$, respectively) (Table 1), while circulating MCP-1 and IL-6 levels were higher in *db/db* mice ($P = 0.021$ and $P = 0.022$, respectively) (Table 1). The expression of tumor necrosis factor alpha (TNF-α) in adipose tissue tended to be higher in *db/db* mice, although this did not reach statistical significance ($P = 0.098$) (Table 1).

In the polygenic diet-induced model, daily energy intake was higher in HFD mice ($P = 0.018$) (Table 1), resulting in greater body mass gain after 20 weeks than in control mice ($P = 0.007$) (Table 1; Fig. 1A). Both subcutaneous ($P = 0.006$) (Table 1) and visceral ($P = 0.013$) (Table 1) adipose tissue depots were larger in HFD mice (Fig. 1C and F), with marked adipocyte hypertrophy (Fig. 1D and G). This was accompanied by ectopic triglyceride accumulation in hepatocytes (Fig. 1E and H) and subsequent enlargement of the liver ($P = 0.016$) (Table 1). HFD mice also had significantly higher circulating levels of cholesterol ($P = 0.006$) and triglycerides ($P = 0.030$) than control littermates (Table 1). Although circulating levels of MCP-1 were comparable between mice ($P = 0.137$) (Table 1), circulating levels of IL-6 ($P = 0.003$) (Table 1) and the expression of TNF-α in SAT were 2-fold higher in HFD mice than in control littermates ($P = 0.033$) (Table 1). Consistent with the development of severe insulin resistance ($P = 0.003$) (Table 1; Fig. 1B), HFD mice developed hyperinsulinemia and hyperglycemia, which are characteristic of clinical T2D (these mice are here referred to as diabetic mice), while control littermates (here referred to as nondiabetic mice) maintained normal glucose homeostasis ($P = 0.016$ and $P = 0.026$, respectively) (Table 1).

Susceptibility to *B. pseudomallei*. The mortality rate for diabetic mice was 40% following subcutaneous infection with *B. pseudomallei* (Fig. 2A). In contrast, all nondiabetic mice survived the 10-day experimental period. At the end of the experimental period, surviving mice were euthanized and necropsied to confirm the establishment of infection, revealing gross abcessation in the livers and spleens of diabetic and nondiabetic mice. Bacteremia was evident in diabetic mice as early as 24 h postinfection ($P = 0.032$) (Fig. 2B), coinciding with increased bacterial loads in the lungs ($P = 0.048$) (Fig. 2B). This was followed by uncontrolled bacterial growth in the spleens of diabetic mice compared to nondiabetic mice by 72 h postinfection ($P = 0.029$) (Fig. 2B). Bacterial loads in the lung also tended to be higher in diabetic mice at 72 h postinfection, though this did not reach statistical significance ($P = 0.069$) (Fig. 2B).

Impaired cytokine expression in diabetic mice. Earlier dissemination of *B. pseudomallei* within 24 h in diabetic mice coincided with reduced expression of proinflammatory cytokines IL-1β ($P = 0.008$), IL-6 ($P = 0.030$) and TNF-α ($P = 0.059$) in SAT compared to that in nondiabetic mice (Fig. 2C). Despite comparable bacterial loads ($P = 0.336$), the expression of T_H1-type cytokines gamma interferon (IFN-γ) ($P = 0.021$) and IL-12 ($P = 0.030$) and subsequent expression of inducible nitric oxide synthase (iNOS) ($P = 0.030$) were similarly reduced in SAT of diabetic mice compared to nondiabetic mice by 24 h postinfection (Fig. 2C).

Exaggerated inflammatory infiltrate in diabetic mice. Despite reduced cytokine expression, inflammatory cell infiltration in SAT was more extensive in diabetic mice at 24 h postinfection (Fig. 3A and D). Cellular infiltration was characterized predominantly by PMN (Fig. 3B and E) and coincided with increased localization of *B. pseudomallei* (Fig. 3C and F). Similarly, the infiltration of PMN was more marked in the spleens of diabetic mice than in those of nondiabetic littermates (Fig. 3G and H).

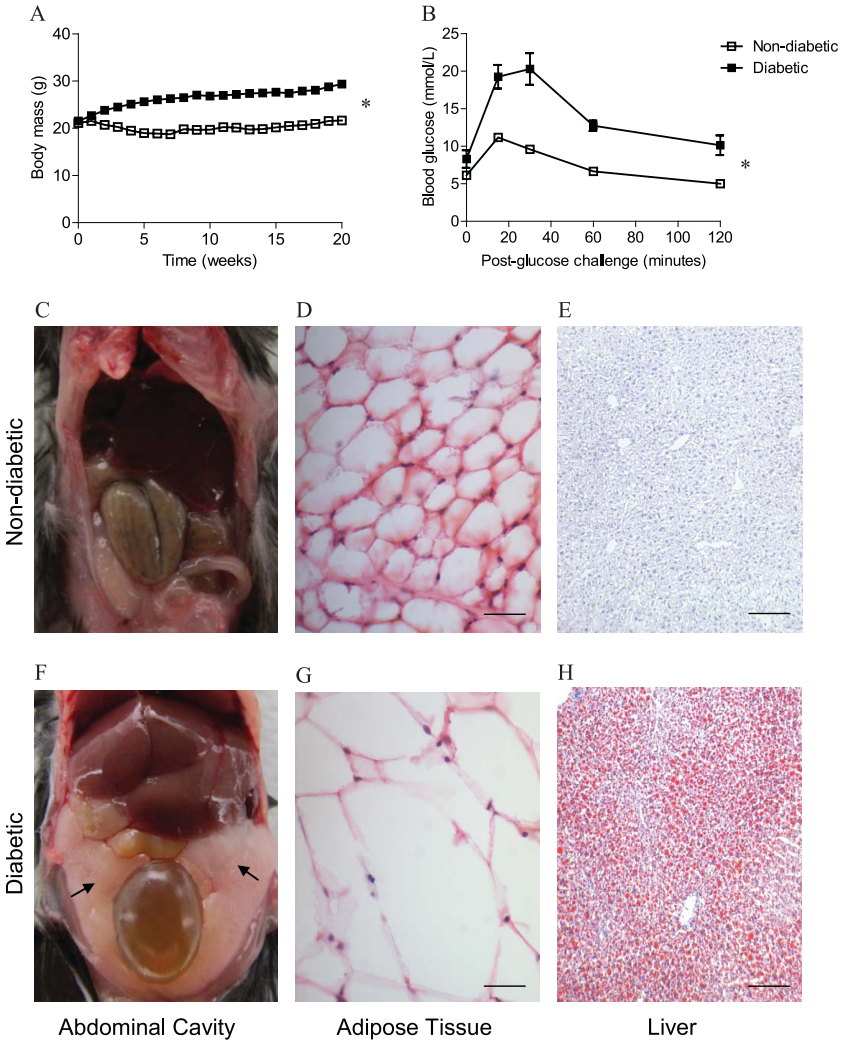

FIG 1 Weight gain and insulin resistance in mice with diet-induced diabetes. (A) Diabetic mice gained significantly more body mass than nondiabetic littermates consuming standard rodent chow. (B) After 20 weeks of diet intervention, diabetic mice were severely insulin resistant following a glucose challenge compared to nondiabetic mice, as evidenced by significantly higher blood glucose levels and delayed glucose clearance. (C to H) Compared to nondiabetic mice (C), visceral adipose tissue depots (arrows) were larger in diabetic mice (F). This was associated with marked adipocyte hypertrophy (G) and hepatic steatosis indicated by oil red O staining (H) in diabetic mice compared to nondiabetic mice (D and E, respectively). Magnifications, ×400 (D and G) and ×100 (E and H). Scale bars, 50 μm (D and G) and 200 μm (E and H). *, $P < 0.05$.

DISCUSSION

The purpose of the current study was to develop and validate a suitable murine model of T2D and melioidosis comorbidity. Leptin signaling-deficient *Dock7*^{m} *Lepr*^{db} mice are a widely used monogenic model of T2D (30). BKS.Cg-*Dock7*^{m} +/+ *Lepr*^{db}/J mice have been used previously as a model for diabetes and comorbid melioidosis (21). However, due to the extensive use of C57BL/6 mice as a model for chronic melioidosis (31), we selected C57BL/6J-*Dock7*^{m} *Lepr*^{db}/++ mice, which were raised on a C57BL/6 background. Homozygous *db/db* mice became severely obese compared to heterozygous *db*/+ littermates due to hyperphagia. Consistent with previous findings, heterozygous *db/db* mice developed insulin resistance as evidenced by impaired glucose clearance and baseline hyperinsulinemia, but the development of hyperglycemia was variable and not statistically significant.

The major caveat for the monogenic model investigated in the current study is the genetic mutation in leptin signaling, which is not the predominant cause of T2D in humans. This could have important implications, since T2D is a polygenic disease with a multifactorial etiology incorporating both genetic and environmental risk factors. Furthermore, leptin is a pleiotropic molecule with extensive metabolic and endocrine functions that are critical to the regulation of both metabolic and immune pathways (32). The effects of leptin signaling deficiency in *db/db* mice extend further than obesity and include abnormal reproductive function, hormonal imbalances, and dysregulation of the hematopoietic and immune systems (32). The use of this model in the study of immune complications related to T2D is therefore limited due to the immune dysregulation afforded by impaired leptin signaling.

We compared this monogenic model to a polygenic model of diet-induced T2D using wild-type C57BL/6 mice. An added advantage of a polygenic model using wild-type C57BL/6 mice, as opposed to the monogenic model discussed above, is the availabil-

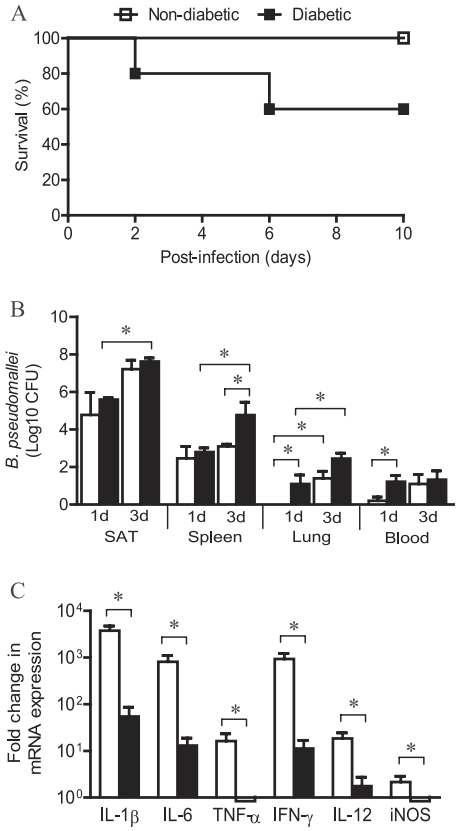

FIG 2 Disease progression following *B. pseudomallei* infection. (A) Following subcutaneous infection with *B. pseudomallei*, the mortality rate in mice with diet-induced diabetes was 40%, compared to 100% survival of nondiabetic mice. (B) Increased mortality of diabetic mice was accompanied by earlier dissemination of *B. pseudomallei* to the blood and lungs within 24 h postinfection compared to that in nondiabetic mice. Between 24 and 72 h postinfection, the bacterial burden significantly increased in diabetic mice at the site of infection and the spleen, leading to a greater bacterial load in the spleen at 72 h postinfection than in nondiabetic mice. The bacterial burden in the lung at 72 h postinfection also tended to be higher in diabetic mice than in nondiabetic mice, although this did not reach statistical significance ($P = 0.069$). (C) Increased dissemination of bacteria in diabetic mice was associated with impaired cytokine expression at the site of infection in subcutaneous adipose tissue (SAT) after 24 h compared to that in nondiabetic mice. *, $P < 0.05$.

ity of a wide variety of knockout genes in the C57BL/6 murine strain, thereby increasing the utility of such a model for future functional studies. Previously, diets with 60% of energy from fat have been used to induce T2D in C57BL/6 mice (33). However, this level markedly exceeds the dietary intake in developed nations (24). Instead, we selected a diet with 40% energy from fat, based on the typical "Western" diet, to more closely reflect dietary intakes in developed nations (24). In this polygenic model, HFD mice gained more body mass than control littermates, which was accompanied by excessive circulating triglyceride and cholesterol levels and marked steatosis due to ectopic fat storage in hepatocytes. This coincided with the development of systemic insulin resistance, followed by elevated blood glucose and delayed glucose clearance in HFD mice.

There is strong evidence that adipose tissue stress due to excessive fat deposition is responsible for the chronic low-grade inflammation that contributes to the pathogenesis of T2D (34, 35). In the current study, the mRNA expression of TNF-α was elevated in the SAT of HFD mice and was accompanied by increased circulating levels of IL-6 compared to those in control littermates. The direct actions of TNF-α and IL-6 on insulin signaling (36, 37) play a critical role in the pathophysiology of T2D (38, 39). We found that the metabolic and biochemical profiles of HFD mice were consistent with the WHO guidelines for diagnostic criteria of T2D (23). Since this model closely reflects the clinical etiopathology of T2D and its associated metabolic complications, it was selected for subsequent experiments to compare disease progression and cytokine expression following infection with *B. pseudomallei*.

Despite an increased incidence of bacterial infections in individuals with T2D, the mechanisms by which T2D can alter the host immune response to a subsequent infection remain poorly characterized. The appropriate timing and regulation of inflammatory cytokines in the early phase of *B. pseudomallei* infection are crucial in determining host resistance (14, 31). Previous studies have established that dissemination of *B. pseudomallei* to the spleen and liver precedes highly elevated levels of IL-1β, IL-6, TNF-α, and IFN-γ at 48 to 72 h, coinciding with overwhelming sepsis and mortality in BALB/c mice (16, 40). This is supported by clinical evidence correlating high serum concentrations of IL-1β, IL-6, TNF-α, IFN-γ, and IL-10 with poor outcome in patients with septic melioidosis (41). Since the hyperinflammatory cytokine response during melioidosis sepsis has been extensively characterized (16, 40, 41), we investigated very early cytokine expression at 24 h postinfection, prior to overt clinical disease and sepsis, to elucidate the mechanisms underlying susceptibility and resistance at the primary site of infection that contribute to increased bacterial dissemination in diabetic mice.

This was the first study comparing inflammatory responses in the first 24 h postinfection at the primary site of infection with *B. pseudomallei* in a diet-induced model of T2D. Interestingly, the increased expression of proinflammatory cytokines in the SAT of diabetic mice prior to infection did not lead to a cumulative increase in the 24 h following *B. pseudomallei* infection. The expression of TNF-α, IL-6, IL-1β, IL-12, IFN-γ, and iNOS in the SAT of diabetic mice was reduced compared to that in nondiabetic mice, despite comparable bacterial loads. This coincided with exaggerated infiltration of inflammatory cells, predominantly PMN, and increased bacterial dissemination to the blood and lungs in diabetic mice, followed by a higher bacterial burden in the spleen.

Our findings suggest that diabetic mice have an inherent inability to contain *B. pseudomallei* at the infection site and a reduced capacity to control the infection once disseminated, compared to nondiabetic mice. The increased susceptibility of diabetic mice to *B. pseudomallei* is consistent with the clinical comorbidity of melioidosis and T2D and highlights the value of this animal model for use in future studies to unravel the mechanisms behind this comorbidity. The use of an *in vivo* animal model has distinct advantages over *in vitro* and *ex vivo* studies, by facilitating investigation of disease progression and local cellular responses within the host in the early stages of infection, prior to the development of overt clinical signs and symptoms.

In parallel with the decreased expression of IFN-γ and IL-12, the expression of iNOS was also significantly reduced in SAT of diabetic mice compared to that of nondiabetic mice at 24 h postinfection. The reduced expression of IL-12, IFN-γ, and iNOS observed in the current study suggests that more severe disease progression in diabetic mice may be due to an impaired activation of phagocytes in the early stages of *B. pseudomallei* infection. This is

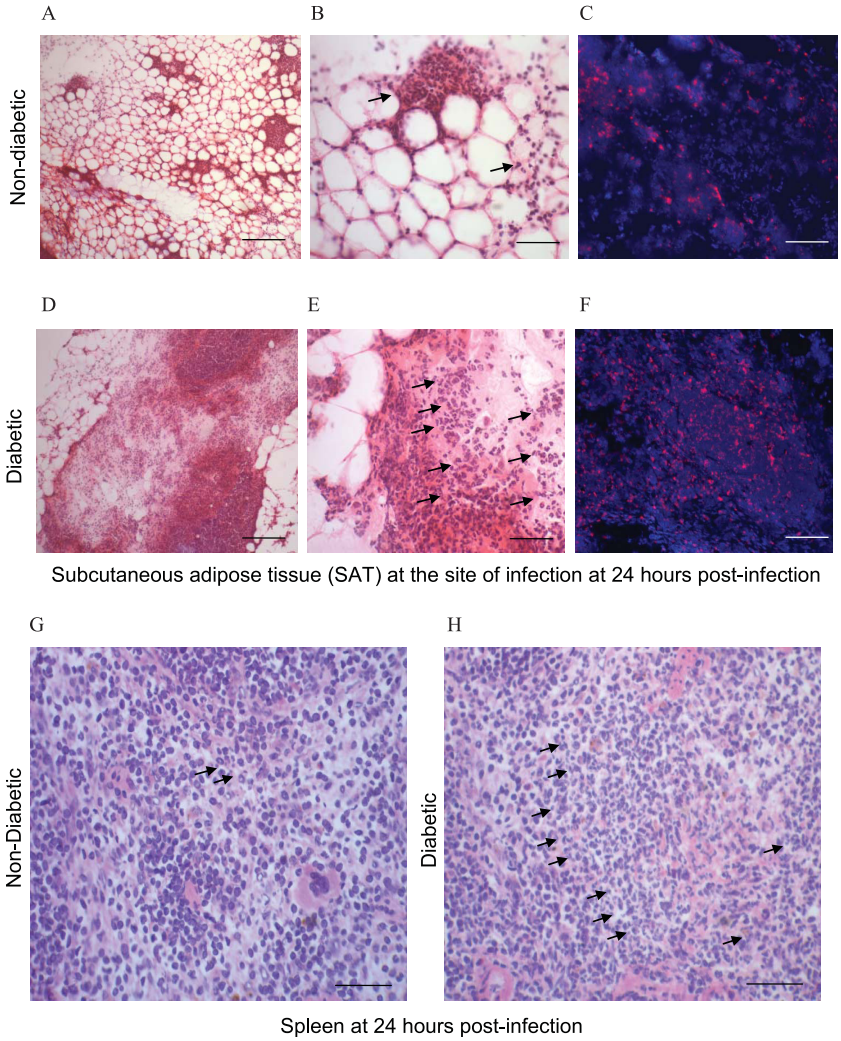

FIG 3 Increased inflammatory infiltrate in mice with diet-induced diabetes. Compared to those in nondiabetic mice (A and B), increased inflammation and recruitment of polymorphonuclear neutrophils (PMN) (arrows) were observed by hematoxylin and eosin staining in SAT of diabetic mice (D and E) at 24 h postinfection. This coincided with increased localization of *B. pseudomallei* (red) in SAT of diabetic mice (F) compared to that in nondiabetic mice (C). Increased inflammation in the spleens of diabetic mice (H) compared to that in nondiabetic mice (G) was also characterized by marked PMN infiltration (arrows). Magnifications, ×100 (A and D), ×400 (B and E), ×200 (C and F), and ×400 (G and H). Scale bars, 200 μm (A and D), 50 μm (B and E), 100 μm (C and F), and 50 μm (G and H).

consistent with the recently described defects in IFN-γ and IL-12 production by peripheral blood mononuclear cells from individuals with T2D after *in vitro* stimulation with *B. pseudomallei* (42). We also observed similar defects in the previously described BKS.Cg-*Dock7*^{m} +/+ *Lepr*^{db}/J diabetic mice, in which reduced levels of nitric oxide (NO) facilitated increased intracellular survival of *B. pseudomallei* in PEC after *in vitro* stimulation (21).

Impaired cytokine responses to *B. pseudomallei* in diabetic mice could be attributed to the reduced activation, recruitment, or functional capacity of macrophages in addition to other phagocytes. In particular, oxidative stress, a significant complication of T2D, interferes with glutathione levels and cellular redox homeostasis, causing damage to macromolecules, signaling, and cell viability (43). Glutathione, an abundant cellular antioxidant, is also critical for regulating many immunological functions (44, 45). A link between reduced glutathione in peripheral blood mononuclear cells from diabetics and impaired IL-12 and IFN-γ production after stimulation with *B. pseudomallei* has been suggested (42). Our ensuing investigations are focused on elucidating the mechanisms underlying the reduced IFN-γ and IL-12 expression observed in diabetic mice in the current study.

Macrophages are an essential component of the protective immune response to intracellular bacteria such as *B. pseudomallei* (31). The depletion of macrophages is associated with increased PMN infiltration and necrosis by 72 h postinfection, and this is similar to the PMN-dominant infiltrate we have described in susceptible BALB/c mice previously (15) and in diabetic mice in the current study. PMN alone are inadequate for an effective immune response against *B. pseudomallei* (31). We hypothesize that impaired macrophage responses lead to a compensatory recruitment of PMN and that this response contributes to focal tissue damage, dissemination, and more severe disease progression in diabetic mice.

In summary, we describe for the first time a polygenic diet-

induced model of T2D and comorbid melioidosis. Compared to the monogenic C57BL/6J-*Dock7*^{m} *Lepr*^{db}/++ mouse model of T2D, the polygenic model described in the current study more closely resembles the etiology and clinical criteria of T2D based on the development of insulin resistance, concomitant dyslipidemia, and overt hyperglycemia. In the current study, we have identified novel differences in early cytokine and cellular responses between diabetic and nondiabetic hosts at the site of infection with *B. pseudomallei*, which could account for the increased bacterial dissemination in individuals with T2D and their greater susceptibility to this tropical disease. Further studies utilizing our model of comorbidity will provide a greater understanding of the mechanisms underlying contrasting immunopathology in hosts with and without T2D.

ACKNOWLEDGMENTS

We thank Ifor Beacham of Griffith University, Australia, for providing the anti-*B. pseudomallei* OMP antibody used in immunofluorescence and Natasha Williams for her technical assistance with the Zeiss laser scanning microscope (LSM 700). We also thank Donna Rudd for her assistance with the biochemical profiling of serum samples.

This work was supported by funding from James Cook University.

REFERENCES

1. **Whiting DR, Guariguata L, Weil C, Shaw J.** 2011. IDF diabetes atlas: global estimates of the prevalence of diabetes for 2011 and 2030. Diabetes Res. Clin. Pract. **94**:311–321.
2. **Koh GC, Peacock SJ, van der Poll T, Wiersinga WJ.** 2012. The impact of diabetes on the pathogenesis of sepsis. Eur. J. Clin. Microbiol. Infect. Dis. **31**:379–388.
3. **White NJ.** 2003. Melioidosis. Lancet **361**:1715–1722.
4. **Suputtamongkol Y, Chaowagul W, Chetchotisakd P, Lertpatanasuwun N, Intaranongpai S, Ruchutrakool T, Budhsarawong D, Mootsikapun P, Wuthiekanun V, Teerawatasook N, Lulitanond A.** 1999. Risk factors for melioidosis and bacteremic melioidosis. Clin. Infect. Dis. **29**:408–413.
5. **Simpson AJ, Newton PN, Chierakul W, Chaowagul W, White NJ.** 2003. Diabetes mellitus, insulin, and melioidosis in Thailand. Clin. Infect. Dis. **36**:e71–e72.
6. **Cheng AC, Currie BJ.** 2005. Melioidosis: epidemiology, pathophysiology, and management. Clin. Microbiol. Rev. **18**:383–416.
7. **Currie BJ, Fisher DA, Howard DM, Burrow JN, Lo D, Selva-Nayagam S, Anstey NM, Huffam SE, Snelling PL, Marks PJ, Stephens DP, Lum GD, Jacups SP, Krause VL.** 2000. Endemic melioidosis in tropical northern Australia: a 10-year prospective study and review of the literature. Clin. Infect. Dis. **31**:981–986.
8. **Currie BJ, Fisher DA, Howard DM, Burrow JNC, Selvanayagam S, Snelling PL, Anstey NM, Mayo MJ.** 2000. The epidemiology of melioidosis in Australia and Papua New Guinea. Acta Trop. **74**:121–127.
9. **Currie BJ, Ward L, Cheng AC.** 2010. The epidemiology and clinical spectrum of melioidosis: 540 cases from the 20 year darwin prospective study. PLoS Negl. Trop. Dis. **4**:e900. doi:10.1371/journal.pntd.0000900.
10. **Limmathurotsakul D, Wongratanacheewin S, Teerawattanasook N, Wongsuvan G, Chaisuksant S, Chetchotisakd P, Chaowagul W, Day NP, Peacock SJ.** 2010. Increasing incidence of human melioidosis in Northeast Thailand. Am. J. Trop. Med. Hyg. **82**:1113–1117.
11. **Saravu K, Mukhopadhyay C, Vishwanath S, Valsalan R, Docherla M, Vandana KE, Shastry BA, Bairy I, Rao SP.** 2010. Melioidosis in southern India: epidemiological and clinical profile. Southeast Asian J. Trop. Med. Public Health **41**:401–409.
12. **Hassan MR, Pani SP, Peng NP, Voralu K, Vijayalakshmi N, Mehanderkar R, Aziz NA, Michael E.** 2010. Incidence, risk factors and clinical epidemiology of melioidosis: a complex socio-ecological emerging infectious disease in the Alor Setar region of Kedah, Malaysia. BMC Infect. Dis. **10**:302.
13. **Chanchamroen S, Kewcharoenwong C, Susaengrat W, Ato M, Lertmemongkolchai G.** 2009. Human polymorphonuclear neutrophil responses to Burkholderia pseudomallei in healthy and diabetic subjects. Infect. Immun. **77**:456–463.
14. **Morris J, Williams N, Rush C, Govan B, Sangla K, Norton R, Ketheesan N.** 2012. Burkholderia pseudomallei triggers altered inflammatory profiles in a whole-blood model of Type 2 diabetes-melioidosis comorbidity. Infect. Immun. **80**:2089–2099.
15. **Barnes JL, Ulett GC, Ketheesan N, Clair T, Summers PM, Hirst RG.** 2001. Induction of multiple chemokine and colony-stimulating factor genes in experimental Burkholderia pseudomallei infection. Immunol. Cell Biol. **79**:490–501.
16. **Ulett GC, Ketheesan N, Hirst RG.** 2000. Proinflammatory cytokine mRNA responses in experimental Burkholderia pseudomallei infection in mice. Acta Trop. **74**:229–234.
17. **Barnes JL, Ketheesan N.** 2005. Route of infection in melioidosis. Emerg. Infect. Dis. **11**:638–639.
18. **Chin CY, Monack DM, Nathan S.** 2012. Delayed activation of host innate immune pathways in streptozotocin-induced diabetic hosts leads to more severe disease during infection with Burkholderia pseudomallei. Immunology **135**:312–332.
19. **Williams NL, Morris JL, Rush C, Govan BL, Ketheesan N.** 2011. Impact of streptozotocin-induced diabetes on functional responses of dendritic cells and macrophages towards Burkholderia pseudomallei. FEMS Immunol. Med. Microbiol. **61**:218–227.
20. **Panchal SK, Brown L.** 2011. Rodent models for metabolic syndrome research. J. Biomed. Biotechnol. **2011**:351982.
21. **Hodgson KA, Morris JL, Feterl ML, Govan BL, Ketheesan N.** 2011. Altered macrophage function is associated with severe Burkholderia pseudomallei infection in a murine model of type 2 diabetes. Microbes Infect. **13**:1177–1184.
22. **Buettner R, Scholmerich J, Bollheimer LC.** 2007. High-fat diets: modeling the metabolic disorders of human obesity in rodents. Obesity (Silver Spring). **15**:798–808.
23. **WHO.** 2003. Report of the expert committee on the diagnosis and classification of diabetes mellitus. Diabetes Care **26**(Suppl. 1):S5–S20.
24. **Cordain L, Eaton SB, Sebastian A, Mann N, Lindeberg S, Watkins BA, O'Keefe JH, Brand-Miller J.** 2005. Origins and evolution of the Western diet: health implications for the 21st century. Am. J. Clin. Nutr. **81**:341–354.
25. **Barnes JL, Ketheesan N.** 2007. Development of protective immunity in a murine model of melioidosis is influenced by the source of Burkholderia pseudomallei antigens. Immunol. Cell Biol. **85**:551–557.
26. **Rozen S, Skaletsky H.** 2000. Primer3 on the WWW for general users and for biologist programmers. Methods Mol. Biol. **132**:365–386.
27. **Wheeler D, Bhagwat M.** 2007. BLAST QuickStart: example-driven web-based BLAST tutorial. Methods Mol. Biol. **395**:149–176.
28. **Pfaffl MW.** 2001. A new mathematical model for relative quantification in real-time RT-PCR. Nucleic Acids Res. **29**:e45.
29. **Vandesompele J, De Preter K, Pattyn F, Poppe B, Van Roy N, De Paepe A, Speleman F.** 2002. Accurate normalization of real-time quantitative RT-PCR data by geometric averaging of multiple internal control genes. Genome Biol. **3**:RESEARCH0034. doi:10.1186/gb-2002-3-7-research0034.
30. **Gilbert ER, Fu Z, Liu D.** 2011. Development of a nongenetic mouse model of type 2 diabetes. Exp. Diabetes Res. **2011**:416254.
31. **Barnes JL, Williams NL, Ketheesan N.** 2008. Susceptibility to Burkholderia pseudomallei is associated with host immune responses involving tumor necrosis factor receptor-1 (TNFR1) and TNF receptor-2 (TNFR2). FEMS Immunol. Med. Microbiol. **52**:379–388.
32. **Fantuzzi G, Faggioni R.** 2000. Leptin in the regulation of immunity, inflammation, and hematopoiesis. J. Leukoc. Biol. **68**:437–446.
33. **Shaul ME, Bennett G, Strissel KJ, Greenberg AS, Obin MS.** 2010. Dynamic, M2-like remodeling phenotypes of CD11c+ adipose tissue macrophages during high-fat diet-induced obesity in mice. Diabetes **59**:1171–1181.
34. **Field AE, Coakley EH, Must A, Spadano JL, Laird N, Dietz WH, Rimm E, Colditz GA.** 2001. Impact of overweight on the risk of developing common chronic diseases during a 10-year period. Arch. Intern. Med. **161**:1581–1586.
35. **Harkins JM, Moustaid-Moussa N, Chung YJ, Penner KM, Pestka JJ, North CM, Claycombe KJ.** 2004. Expression of interleukin-6 is greater in preadipocytes than in adipocytes of 3T3-L1 cells and C57BL/6J and ob/ob mice. J. Nutr. **134**:2673–2677.
36. **Hotamisligil GS.** 2006. Inflammation and metabolic disorders. Nature **444**:860–867.
37. **Bastard JP, Maachi M, Lagathu C, Kim MJ, Caron M, Vidal H, Capeau**

J, Feve B. 2006. Recent advances in the relationship between obesity, inflammation, and insulin resistance. Eur. Cytokine Netw. **17**:4–12.
38. **Galic S, Oakhill JS, Steinberg GR.** 2010. Adipose tissue as an endocrine organ. Mol. Cell. Endocrinol. **316**:129–139.
39. **Schaffler A, Scholmerich J.** 2010. Innate immunity and adipose tissue biology. Trends Immunol. **31**:228–235.
40. **Ulett GC, Ketheesan N, Hirst RG.** 2000. Cytokine gene expression in innately susceptible BALB/c mice and relatively resistant C57BL/6 mice during infection with virulent Burkholderia pseudomallei. Infect. Immun. **68**:2034–2042.
41. **Wiersinga WJ, Dessing MC, Kager PA, Cheng AC, Limmathurotsakul D, Day NP, Dondorp AM, van der Poll T, Peacock SJ.** 2007. High-throughput mRNA profiling characterizes the expression of inflammatory molecules in sepsis caused by Burkholderia pseudomallei. Infect. Immun. **75**:3074–3079.
42. **Tan KS, Lee KO, Low KC, Gamage AM, Liu Y, Tan GY, Koh HQ, Alonso S, Gan YH.** 2012. Glutathione deficiency in type 2 diabetes impairs cytokine responses and control of intracellular bacteria. J. Clin. Invest. **122**:2289–2300.
43. **Ryter SW, Kim HP, Hoetzel A, Park JW, Nakahira K, Wang X, Choi AM.** 2007. Mechanisms of cell death in oxidative stress. Antioxid. Redox Signal. **9**:49–89.
44. **Fraternale A, Paoletti MF, Dominici S, Caputo A, Castaldello A, Millo E, Brocca-Cofano E, Smietana M, Clayette P, Oiry J, Benatti U, Magnani M.** 2010. The increase in intra-macrophage thiols induced by new pro-GSH molecules directs the Th1 skewing in ovalbumin immunized mice. Vaccine **28**:7676–7682.
45. **Murata Y, Shimamura T, Hamuro J.** 2002. The polarization of T(h)1/T(h)2 balance is dependent on the intracellular thiol redox status of macrophages due to the distinctive cytokine production. Int. Immunol. **14**:201–212.